Eur. Phys. J. D **21**, 73–81 (2002)
DOI: 10.1140/epjd/e2002-00179-x

THE EUROPEAN PHYSICAL JOURNAL D

Axial emission profiles and apparent secondary electron yield in abnormal glow discharges in argon

D. Marić[1], K. Kutasi[2], G. Malović[1], Z. Donkó[2,a], and Z.Lj. Petrović[1]

[1] Institute of Physics, P.O.B. 68, 11080 Zemun, Belgrade, Yugoslavia
[2] Research Institute for Solid State Physics and Optics, Hungarian Academy of Sciences, P.O.B. 49, 1525 Budapest, Hungary

Received 21 May 2002
Published online 24 September 2002 –

Abstract. This paper reports investigations of argon glow discharges established between flat disk electrodes, at pressure × electrode separation values between 45 Pa cm and 150 Pa cm. Parallel to the experimental studies the discharge is also described by a self-consistent hybrid model. The model uses as input data the measured electrical characteristics, this way making it possible to determine the apparent secondary electron emission coefficient. The model is verified through comparison of the measured and calculated spatial profiles of light emission, which are in good agreement for a wide range of conditions in the abnormal glow mode. Additionally, we investigate the dependence of the field reversal position on the discharge conditions and test the usual assumption that the position of the peak of emission closely coincides with the cathode fall – negative glow boundary.

PACS. 51.50.+v Electrical properties (ionization, breakdown, electron and ion mobility, etc.) – 52.65.-y Plasma simulation – 52.80.Hc Glow; corona

1 Introduction

Townsend's theory of low pressure breakdown and low current dark discharges has recently been revised to include space charge effects [1,2] and feedback mechanisms other than production of electrons by ion impact at the cathode [3]. Careful and well defined measurements in the dark Townsend regime [4–9] led to re-analysis of the role of different (surface and gas-phase) elementary processes in electron/ion production in gas breakdown and in the maintenance of self-sustained discharges. In particular it has been established that the secondary electron yield at the surface of the cathode depends on the mean energy of ions hitting the surface. The ion energy is affected by the external voltage, by the local reduced electric field E/n (where E is the electric field and n is the gas number density) and also by the current which leads to a perturbation of the field mostly in front of the cathode. It has also been shown that this weak dependence of the secondary yield on the space charge perturbation to the field, associated with the strong dependence of the ionization coefficient on E/n near the operating point, causes the negative differential resistance that has been observed in low-current Townsend discharges [1]. Extension of Townsend's theory developed on the basis of local-field approximation by Phelps and coworkers [1,2] was shown to be quite successful and it gave a good agreement with the experimental results for field distributions (based on the local field approximation) [10].

On the other hand it was found that, at least for the case of argon, a large number of processes participate in secondary electron production at the cathode (see [3] and references therein). As a matter of fact ions dominate in a very narrow range of conditions *i.e.* only for moderately high E/n. Thus a new series of measurements of the breakdown conditions that may be analyzed by including the new understanding of the processes on the cathode and of the non-equilibrium effects near the cathode [11] has been undertaken to provide the basis for the re-analysis of the secondary electron yield data [11–14]. Phelps and Petrović have shown [3] that application of the secondary electron yield data obtained by ion beams under high vacuum conditions for gas discharge modeling is not appropriate, even though most of the modeling of collisional plasmas and gas discharges is based on the ion beam data whereby a constant value of typically 0.08 for argon [15] is assumed.

At the same time significant advances in discharge modeling have been made in the past 10 years especially with the development of hybrid codes that combine the kinetic simulation of fast electrons with the computationally effective fluid treatment of slow electrons and ions [16–20]. Hybrid models are able to deal with the spatial nonlocality of the electron transport in the cathode sheath and have provided important information about the phenomena taking place in a wide variety of discharges [16–21].

[a] e-mail: donko@sunserv.kfki.hu

The need for secondary yield values for modeling is due to the fact that with the knowledge of γ the electrical characteristics of the discharge can be calculated. Hybrid codes, usually assuming a constant value for γ, have successfully been applied in studies of glow discharges [16–21]. In order to further improve the accuracy of these models it was justified to address the question whether application of secondary electron yields obtained for low-current discharge conditions (*i.e.* homogeneous field) [3] would yield satisfactory results in the region of the normal (constricted) glow and abnormal (high current diffuse) glow. This test, however, resulted in non-physical behavior of the electrical characteristics (negative differential resistance in the abnormal glow mode) [22] – mainly caused by a different combination and properties of different feedback mechanisms resulting from significantly different field and space charge distributions. Further on, using energy-dependent secondary yield values for argon ions and fast atoms, the apparent γ has recently been derived for cathode-fall conditions, from a heavy-particle hybrid model [23]. The γ values obtained in this study have been found to be significantly lower compared to the case of the homogeneous field [3] and to change remarkably with changing discharge conditions. This implies that it is generally difficult to prescribe a certain value of γ which describes the discharge correctly for a wide range of operating conditions. As an alternative approach – due to the lack of reliable experimental secondary yield values for different gas – cathode material combinations –, γ has been used as a fitting parameter in some of the recent modeling studies, it has been adjusted at the different discharge conditions to match the calculated electrical characteristics with the experimental ones [24,25].

All the dc and low frequency glow discharges operate under conditions when secondary electron production at the cathode surface is the key mechanism in discharge maintenance. At the same time practical rf plasmas [26] are used under conditions where high power operation requires predominance of the secondary electron production at the surface of the temporary cathode. Thus it is our motivation to extend the understanding of secondary electron production to high current non-equilibrium discharges such as the abnormal glow.

Both from the point of view of deeper understanding of the physics of gas discharges and from the point of view of their applications there is a strong need for the development of accurate discharge models. At the same time the verification of the models – which is also highly desirable – can be done only on the basis on reliable experimental data. Therefore, in this paper, besides presenting the results of modeling calculations, we make comparison between experimental and calculated axial profiles of emission which provide detailed understanding of the anatomy of the discharge [5,10,27,28].

The paper is structured as follows. Section 2 describes the experimental set-up, while the simulation model is outlined in Section 3. Section 4 presents the experimental and modeling results, and their comparison. Our work is summarized in Section 5.

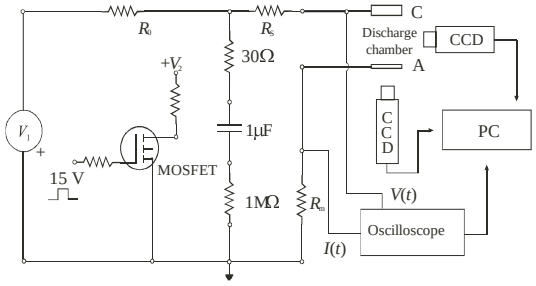

Fig. 1. Simplified schematics of the experimental set-up and the electrical circuit.

2 Experimental

The schematics of the experimental set-up is shown in Figure 1. The discharge vessel used in our experiment consists of parallel plane electrodes tightly fitting inside a quartz cylinder which prevents long-path breakdown. The cathode (C) is made of copper and the anode (A) of quartz with a transparent yet conductive thin film of platinum deposited on top of it. The diameter of the electrodes is 5.4 cm. The distance between the two electrodes may be adjusted by fixed electrode supports but in this experiment we keep the distance at $d = 1.1$ cm.

The system is pumped down to a base pressure of below 10^{-6} torr and a very small flow of gas (argon in this case) is used to reduce the accumulation of impurities. Prior to the measurements, the surface of the cathode is treated by a relatively high current discharge in hydrogen (30 μA) until a stable breakdown voltage is achieved (approximately 30 minutes).

Our system has a facility (see Fig. 1) for producing a pulse of current in addition to a very small dc current [8,10]. The dc current is used to reduce the breakdown delay time, and is as small as possible (typically 1–2 μA) in order to reduce heating and conditioning of the cathode during the measurements. The voltage is measured by two probes, one at the cathode and the other in the anode circuit. The second probe is used only when a relatively high monitoring resistor is connected into the low-voltage anode circuit to determine the current. Pulses of higher current last usually only long enough ($\tau = 2$ ms) to make a reliable recording of voltage and current transients. For the recordings of the axial intensity profiles the length of the pulse is somewhat extended ($\tau = 10$ ms) so that the emission profiles recorded by the CCD camera correspond to the conditions of the pulse, not to the dc current.

Recordings of axial and radial emission profiles are made by a cooled CCD camera (type: Electrim EDC1000) sensitive mostly in the red part of the spectrum. While we do not measure absolute values of the intensity, relative relationships between the emission profiles at different currents are established by making recordings under identical conditions for two different openings of the aperture. Thus we can be sure that saturation of the recorded emission signal is not reached.

Measurements are made in pure argon at pressure (p)$\times$ gap (d) products of $pd = 150$ Pa cm, 75 Pa cm and

45 Pa cm (corresponding approximately to pressures of 1 torr, 0.5 torr and 0.3 torr). Besides the measurement of the volt-ampere characteristics of the discharges and the axial emission profiles we also measure radial profiles of emission through the transparent anode to obtain information about the radial structure of the discharge.

3 Hybrid model

Our one-dimensional hybrid model combines fluid description of positive ions and slow electrons with Monte Carlo (MC) simulation of fast electrons [16–20]. The fluid model is based on the continuity equations and the Poisson equation:

$$\frac{\partial n_{\mathrm{e(i)}}}{\partial t} + \frac{\partial (n_{\mathrm{e(i)}} v_{\mathrm{e(i)}})}{\partial x} = S_{\mathrm{e(i)}}, \tag{1}$$

$$\Delta V = -\frac{e}{\epsilon_0}(n_{\mathrm{i}} - n_{\mathrm{e}}), \tag{2}$$

where $n_{\mathrm{e(i)}}$ are the densities, $v_{\mathrm{e(i)}}$ are the mean velocities, and $S_{\mathrm{e(i)}}$ are the source functions of the slow electrons and ions, respectively, V is the electrostatic potential, e is the elementary charge, and ϵ_0 is the permittivity of free space. The space charge created by the fast electrons – being several orders of magnitude smaller than that created by the slow electrons – is neglected in (2). The mean velocities are calculated from the momentum transfer equations:

$$\Phi_{\mathrm{e(i)}} = n_{\mathrm{e(i)}} v_{\mathrm{e(i)}} = s n_{\mathrm{e(i)}} \mu_{\mathrm{e(i)}} E - \frac{\partial (n_{\mathrm{e(i)}} D_{\mathrm{e(i)}})}{\partial x}, \tag{3}$$

where $s = -1$ for electrons and $s = 1$ for ions, $\mu_{\mathrm{e(i)}}$ and $D_{\mathrm{e(i)}}$ are the mobility and diffusion coefficients of electrons (ions) and $\Phi_{\mathrm{e(i)}}$ are the corresponding fluxes. The mobility of electrons in argon is $\mu_{\mathrm{e}} = 3 \times 10^5/p$ cm^2 V^{-1} s^{-1} (p is given in torr) [29], the mobility of the argon ions is taken from [3]. The diffusion coefficient of electrons is chosen to be $D_{\mathrm{e}} = kT_{\mathrm{e}}\mu_{\mathrm{e}}$ with $kT_{\mathrm{e}} = 0.1$ eV characteristic energy assigned to the slow electron group. The diffusion coefficient of argon ions in argon is $D_{\mathrm{i}} = kT_{\mathrm{i}}\mu_{\mathrm{i}}$ with $kT_{\mathrm{i}} = 0.026$ eV (corresponding to a gas temperature of 300 K).

The sources of ions and slow electrons are calculated from the MC simulation, which traces the fast electrons. In our calculation we take into account the elastic scattering of electrons from argon atoms, electron impact excitation and ionization of argon atoms. The cross-sections of these elementary processes are taken from reference [30]. The ionization source function $S_{\mathrm{i}}(x)$ is accumulated from the individual ionization processes. The electrons are transferred to the slow electron group (through the $S_{\mathrm{e}}(x)$ source function) when their (kinetic + potential) energy falls below the excitation energy of the argon atoms.

After completing the MC simulation cycle the ion and slow electron source functions, $S_{\mathrm{e}}(x)$ and $S_{\mathrm{i}}(x)$, which serve as the input to the next fluid cycle, are normalized by the actual value of the current I (calculated in the previous fluid cycle):

$$S(x) = \frac{I}{e(1+1/\gamma)\Delta V_x}\frac{N_x}{N_0}, \tag{4}$$

where N_0 is the number of primary electrons emitted from the cathode in the simulation, N_x is the number of ions (slow electrons) created in a cell of ΔV_x volume around x, and γ is the apparent secondary electron yield.

The fluid equations are solved on a uniform grid containing 200 points. The boundary conditions at the walls are zero density of particles and prescribed values of the potential (zero at the cathode and V at the anode). The fluid equations are solved using an implicit integration scheme [16] with a typical integration time step of the order of 10 ns.

The apparent secondary electron emission coefficient is taken as a variable (fitting) parameter. In the iterative solution of the fluid and MC models γ is adjusted "automatically" to obtain a current density converging to the experimental value [24,25]. In the simulations we neglect the heating of the gas and recombination processes, justified by the low electrical input power to the discharge and by the low pressure, respectively. On the other hand, we include the backscattering of electrons from the anode, with a reflection coefficient of 0.4 [31], and a fractional energy loss of 0.5 [32].

In our calculations we assume that the spatial distribution of the light intensity is proportional to the (total) electron impact excitation rate, calculated from the fast-electron Monte Carlo model. Our method of calculation is justified by studies of plane-cathode Ar glow discharges, based on a hybrid + collisional-radiative model [33], which have shown that the majority of spectral lines (excited by electron impact) exhibit very similar spatial intensity distribution.

More details about the simulation procedures can be found in *e.g.* [24,25].

4 Experimental and theoretical data and their comparisons

4.1 Experimental results

The volt-ampere characteristics of the discharges at different *pd* values are shown in Figures 2a–2c. The data are in good agreement with the earlier measurements of volt-ampere characteristics at lower currents and with the measurements of negative differential resistances [2,6,8]. The different symbols in Figures 2a–2c correspond to different values of resistances in the external electrical circuit (see Fig. 1). At all three values of *pd* the volt-ampere curves exhibit a negative slope at low currents. Having passed the minimum maintaining voltage there is a distinct growth of voltage with the current, corresponding to the abnormal (high current diffuse) glow regime. Even though there have been small fluctuations of the dc breakdown voltage, the volt-ampere characteristics – shown as the difference of the actual discharge voltage and the voltage measured at low current (breakdown limit) – are in excellent agreement from one data set to another and have been reproducible throughout the period of measurements.

The spatial profiles of emission at lower currents, covering the Townsend's (low current diffuse) regime have

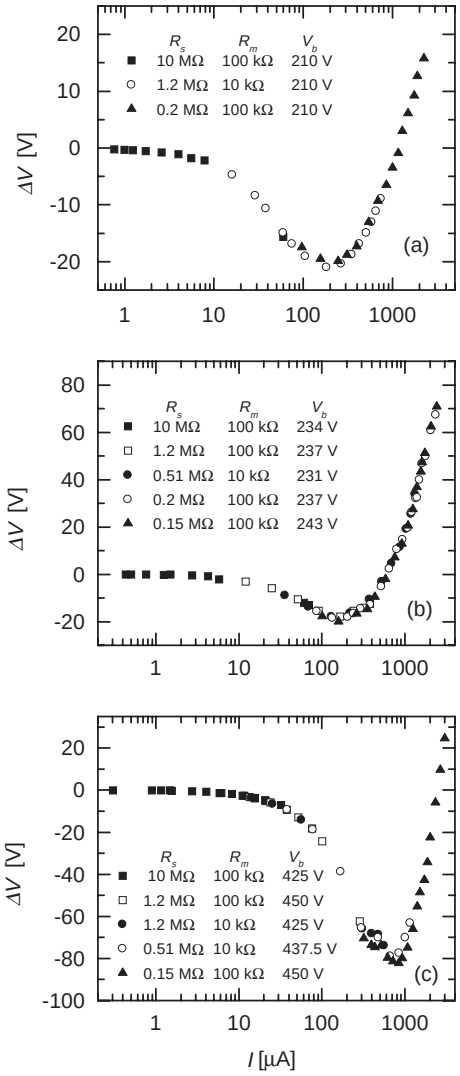

Fig. 2. Volt-ampere characteristics for low current discharges in argon for different values of *pd*: (a) 150 Pa cm, (b) 75 Pa cm, and (c) 45 Pa cm, at $d = 1.1$ cm. The different symbols represent different values of the circuit impedances R_s and R_m (see Fig. 1), V_b denotes the breakdown potential. The plots show the difference of the actual discharge voltage and the breakdown (low current limit) voltage, allowing small variations of the breakdown voltage due to conditioning of the cathode surface during the experiment.

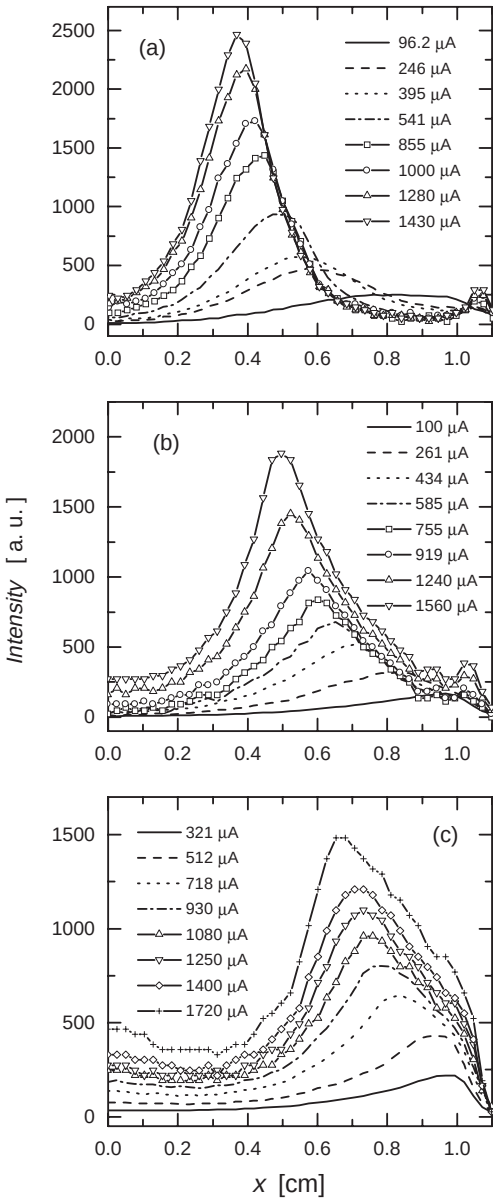

Fig. 3. Axial profiles of emission for three different values of *pd*: (a) 150 Pa cm, (b) 75 Pa cm, and (c) 45 Pa cm. The cathode is situated at $x = 0$ and the anode position is $x = 1.1$ cm.

been studied in our previous papers [10,34]. These profiles clearly exhibit an exponential growth at very low currents. At somewhat higher currents below the transition to the normal (constricted) glow the growth can be described by a gradually changing exponent. It has even been possible to apply the local field approximation and to obtain the spatial profile of field from the well known dependence of the ionization coefficient on E/n [10]. In this paper (see Figs. 3a–3c) we start from higher currents at the beginning of the normal glow ($\approx$100 μA). At the lowest currents concerned here we observe a continuous growth of emission towards the anode. As the current increases the peak of emission gradually moves away from the anode, while the peak intensity increases. Especially at the highest pressure (Fig. 3a), the ionization coefficient drops down towards the anode, while at the lowest pressure (Fig. 3c) there is a distinct non-equilibrium region without the growth of emission, close to the cathode.

Assuming that the position of the emission peak matches the position of the cathode sheath – negative glow boundary, the present data allow us to determine the length of the cathode sheath and to establish its dependence on current and pressure.

It is noted that measurements performed for the same current at two different circuit impedances are in excellent agreement both in terms of volt-ampere characteristics and in terms of spatial emission profiles.

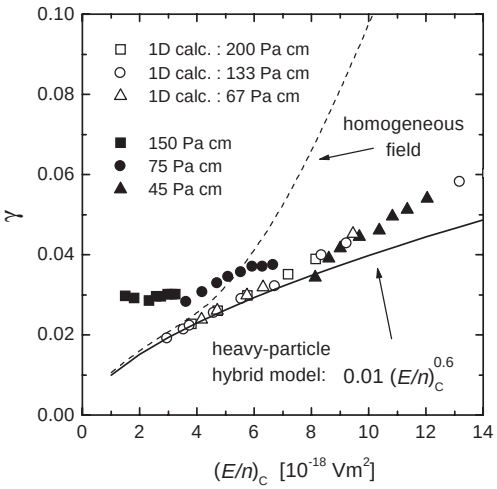

Fig. 4. Calculated apparent secondary electron emission coefficient as a function of the reduced field at the cathode. Solid symbols: results of the present calculations, open symbols: previous calculations of γ with a one-dimensional electron-ion hybrid model [23], (——): heavy-particle hybrid calculations [23], (- - - -): homogeneous field data [3].

4.2 Modeling results

The values of the apparent secondary yield γ (determined by the fitting procedure described in Sect. 3) are shown in Figure 4 for all *pd* values investigated. Figure 4 also shows the secondary yield values obtained by Phelps and Petrović [3] for homogeneous field, as well as the γ values calculated by Donkó [23] for cathode-fall conditions. These latter calculations of γ (based on the flux-energy distributions of heavy particles obtained from a one-dimensional heavy-particle hybrid model) have shown that (i) the apparent secondary yield is a function of the reduced electric field at the cathode, $(E/n)_c$, and can be given as $\gamma \approx 0.01(E/n)_c^{0.6}$ in the 3–20 kTd range of $(E/n)_c$ (1 Td = 10^{-17} V cm^2) and that (ii) the results show little sensitivity on the pressure × electrode gap product [23]. The functional relation given above has also been confirmed to hold at even higher $(E/n)_c$ values by subsequent simulations of Bogaerts and Gijbels of an argon discharge in an analytical glow discharge cell [35].

Apart from the ion-induced electron emission from the cathode, the heavy-particle hybrid models also include fast atom-initiated electron emission from the cathode and production of ions by fast ion/atom + Ar atom collisions (heavy-particle ionization). Although the relative amount of ionization by heavy particles is relatively small, this additional ionization source is still important as the ionization occurs mainly near the cathode, and the electrons created in these processes behave almost like the electrons emitted from the cathode (*i.e.* they give rise to avalanches). Neglecting these processes – like it is done in electron-ion hybrid models – a decreased ionization rate and consequently a smaller current is obtained at fixed voltage [23]. Thus, in an electron-ion hybrid model a somewhat higher γ has to be used to reproduce the electrical characteristics calculated by the heavy-particle model.

The present data show excellent agreement at high $(E/n)_c$ (*i.e.* at low *pd*) with the earlier values of γ calculated from an electron-ion hybrid model, as it can be seen in Figure 4. While the earlier calculations show that in the low $(E/n)_c$ limit the calculated γ [23] approaches the results of Phelps and Petrović [3], the data determined from the present measurements of the electrical characteristics are higher than this, in the low $(E/n)_c$ limit we find now $\gamma \approx 0.03$. Such a difference is acceptable as the secondary electron emission coefficient and the relative importance of different surface processes contributing to electron emission depend strongly on the surface conditions of the cathode [3,36]. In the present experiment special care has been taken to make the measurements reproducible by a standard procedure of pre-measurement conditioning of the cathode. However, the cathode conditions obtained this way may not be the same as those in other experiments. The calculations in [23] have been carried out for cathode surfaces under "laboratory conditions" (or "dirty" surfaces as compared to ultra-high vacuum conditions). The differences found here may be due to a cleaner cathode surface in the present measurements compared to that in some other experiments. Finally we note that at high $(E/n)_c$ our data lie well below the apparent γ values for homogeneous field (low current Townsend, or breakdown) conditions [3], in agreement with the findings of [23].

The spatial profiles of the electric field, ion density as well as electron density are plotted in Figures 5a and 5b (for 150 Pa cm) and in Figures 6a and 6b (for 45 Pa cm). For almost all discharge conditions we find a linear decay of the electric field in the cathode sheath, except at the lower values of the current, at the higher *pd* value (150 Pa cm). In this range of discharge conditions we are in, or near the normal glow mode, where the two-dimensional structure of the discharge is important and thus our one-dimensional model does not describe the discharge accurately. For these conditions the electron and ion density profiles are also unusual, we either do not observe the accumulation of ions at the anode side of the discharge at all, or the ion space charge in this region is below that found in the cathode sheath. At the lower *pd* value (45 Pa cm), we observe the usual density profiles as shown in Figure 6b. The ion density in the sheath is in the order of 4–8 × 10^8 cm^{-3} and the density in the negative glow rises up to 4 × 10^{10} cm^{-3} at the highest current. The density of electrons is appreciable only in the negative glow, in that region the electron density is nearly equal to the ion density. The electron density rises sharply at the cathode sheath – negative glow boundary. This is explained by the fact that the negative space charge is made up of slow electrons which accumulate in the potential well formed in the negative glow region and they cannot diffuse back to the cathode sheath due to the increasing electric field towards the sheath.

The reversal of the electric field can clearly be observed within the abnormal glow operating conditions: at a certain position in the negative glow the electric field changes sign and tends to confine the electrons in the negative glow plasma meanwhile driving some of the ions towards the

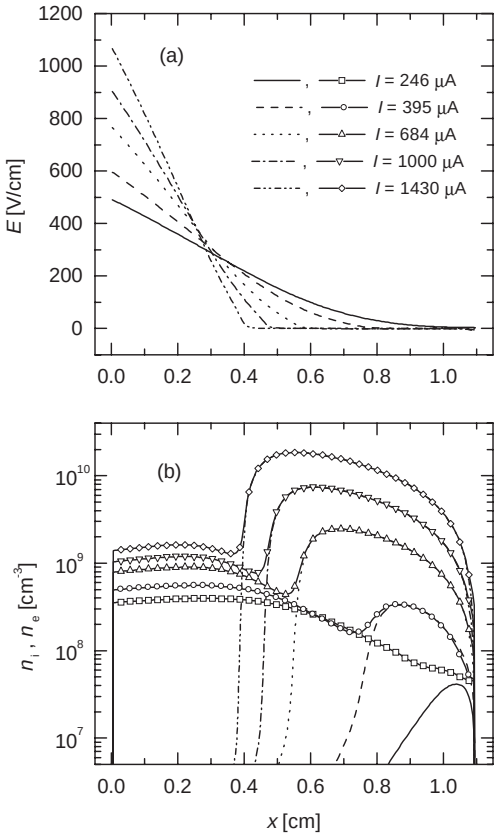

Fig. 5. Calculated discharge characteristics for $pd = 150$ Pa cm at different discharge currents: (a) electric field distribution, (b) ion density (lines + symbols) and electron density (lines).

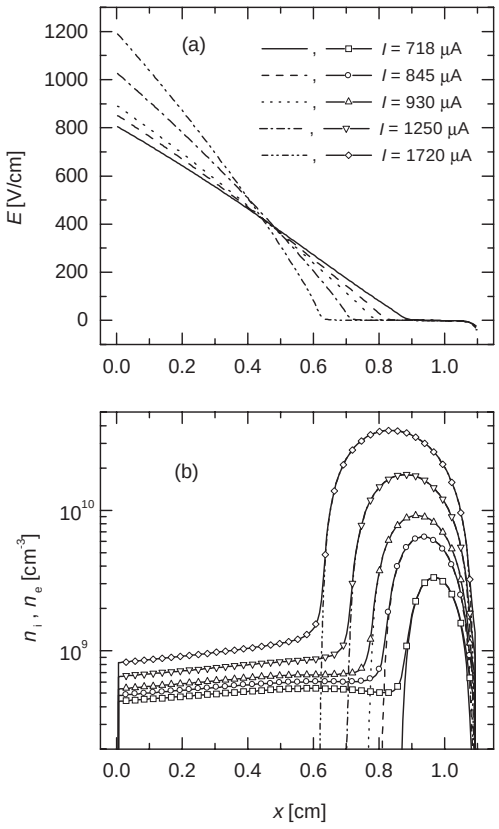

Fig. 6. Calculated discharge characteristics for $pd = 45$ Pa cm at different discharge currents: (a) electric field distribution, (b) ion density (lines + symbols) and electron density (lines).

anode. According to the simple analytical model of Boeuf and Pitchford [37] the position of the field reversal, d_f depends only on the electrode distance d, the length of the cathode sheath d_c and the energy relaxation length of the fast electrons λ:

$$\frac{d_f - d_c}{d - d_c} = -\Lambda \ln\left[\Lambda(1 - e^{-1/\Lambda})\right] \qquad (5)$$

where $\Lambda = \lambda/(d - d_c)$.

In [37] it has been shown that at small relaxation lengths (when the electrode gap is much larger than the length of the sheath) the field reversal position is close to the sheath-glow boundary. At longer relaxation lengths of the fast electrons, *i.e.* towards the obstructed discharge mode, the field reversal point moves towards the mid-position between the sheath-glow boundary and the anode. In Figure 7 we compare the analytical results for the field reversal position (5) with our hybrid modeling data. The energy relaxation length of the electrons have been determined from the decay of the calculated excitation rate beyond the peak intensity of the negative glow. The field reversal positions obtained from the hybrid model are in excellent agreement with the predictions of the model of Boeuf and Pitchford. The data clearly show the shift of d_f towards the anode as pd decreases. It is interesting to note that $\lambda/(d - d_c)$ is nearly constant at a constant pd and d_f changes slightly with changing current (and voltage).

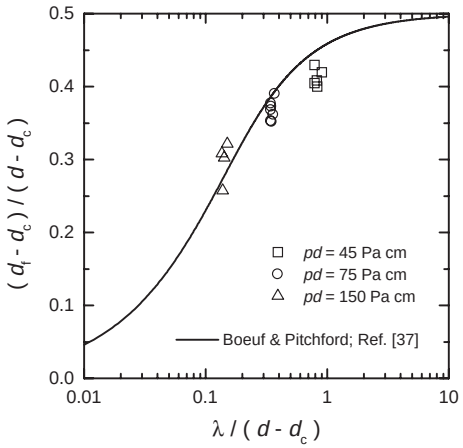

Fig. 7. Dependence of the field reversal position d_f on discharge conditions: (——) analytical model of reference [37], symbols: present hybrid modeling data.

4.3 Axial emission profiles

The critical comparison of the experimental and theoretical data may be obtained from the axial profiles of emission. Since our experimental intensity data are not absolute values, we normalize the calculated and experimental data at one pair of current and pressure values and compare the ratios of all other profiles.

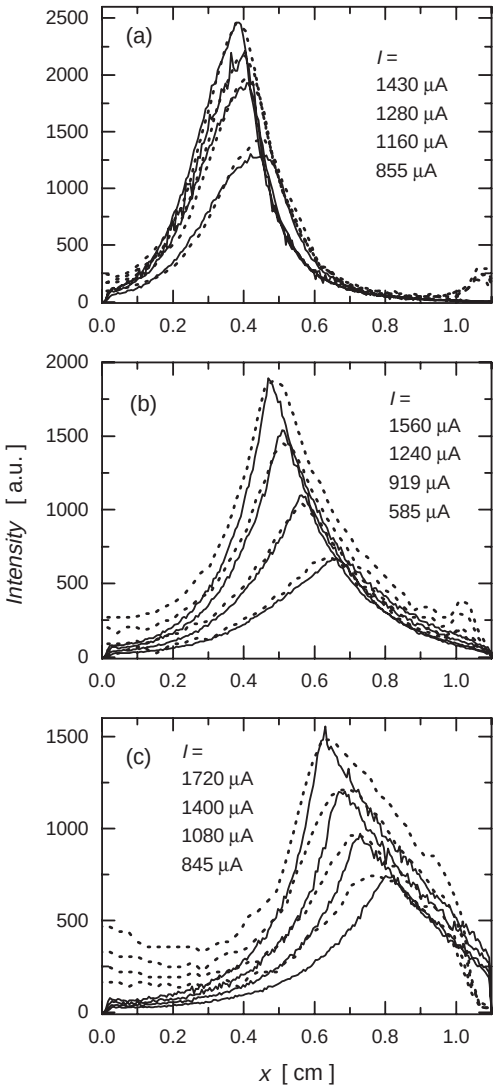

Fig. 8. Measured (- - - -) and the calculated (——) light intensity distributions for selected values of discharge current I, at (a) $pd = 150$ Pa cm, (b) $pd = 75$ Pa cm, and (c) $pd = 45$ Pa cm conditions.

The comparison of the measured and calculated intensity distributions for selected values of currents and for three values of pd are presented in Figures 8a–8c. In all cases shown there is an excellent agreement between the measured and calculated profiles both in terms of shape and relative magnitude of the negative glow. Correspondingly, the peaks of emission agree very well and so does the dependence of the position of the peak with the current. We also reproduce broadening and skewing of the negative glow as the pressure is decreased. Showing more than four different currents per graph would make it impossible to compare the data but the agreement is equally good in all cases, except for high pd, low-current conditions (see later). The relatively low intensity signal in the cathode fall region may originate from heavy-particle excitation of spectral lines (see *e.g.* [28]), and it is not reproduced by the calculations as such processes are not included in the present model.

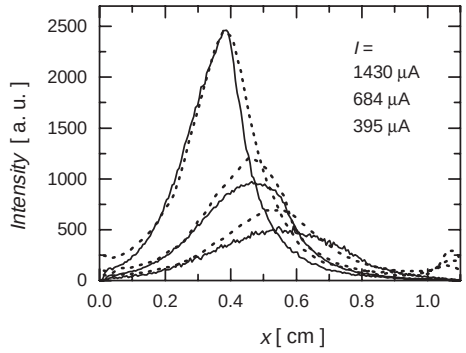

Fig. 9. Experimental (- - - -) and calculated (——) axial profiles of emission for three different currents at $pd = 150$ Pa cm. One higher and two lower currents are shown here to illustrate the discrepancy occurring in the constricted regime.

The only set of conditions when the agreement between the measured and calculated distributions is less perfect is at $pd = 150$ Pa cm (*i.e.* at the highest pressure) and at the lower currents covered here, where we have a disagreement in magnitudes of emission peaks up to a factor of two. This is shown in Figure 9, for two values of current together with one higher value of current for comparison. Such discrepancy does not occur for other pressures even at the lowest currents. The explanation for this disagreement may be reached by considering the fact that the currents where the discrepancy occurs are at the edge of the normal glow region. Thus one may expect that at such high pressure the constriction of the discharge is significant. Correspondingly, our one-dimensional model fails to represent the actual field distribution, and consequently the emission rates which are very sensitive to the electron energy are affected considerably. The same argument may be used to explain the charged particle and field profiles under the same conditions (see Fig. 5). The observations made through the transparent electrode indeed confirm that for the currents where discrepancy between the measured and calculated axial profiles occurs, a marked constriction is observed, where the discharge covers less than 50% of the cathode area. At lower pressures the constriction is not so pronounced so the discharge is more "one-dimensional" even at low currents and thus our one-dimensional model describes the discharge more accurately.

4.4 The thickness of the cathode fall

Finally we address the issue of the width of the cathode fall region. It is often assumed that the position of the maximum of emission corresponds to the edge of the cathode fall. The argument is based on a simple consideration of the electron energy and multiplication kinetics, that may not be accurate under the entire range of realistic conditions. In the following we compare (i) the position of the emission maxima in the experiment, (ii) the theoretical emission maxima calculated from the Monte Carlo

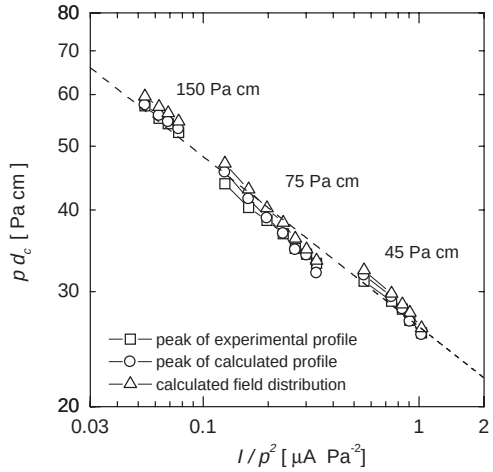

Fig. 10. Width of the cathode sheath (d_c) determined from the experimental and simulated profiles as well as from the axial field distribution. The dashed line indicates a scaling of pd_c with the reduced discharge current I/p^2.

simulation and (iii) the position of the cathode sheath – negative glow boundary as obtained from a linear extrapolation of the calculated electric field to zero value. The results for all the discharge conditions covered here are plotted in Figure 10.

The experimental position of the emission peak, the theoretical emission peak and the width of the cathode fall extrapolated from the field distribution, for the three *pd* values are in a very good agreement, that is well within the experimental uncertainty of the position. One should bear in mind that initially there was a systematic shift of emission peaks of much less than 0.1 cm which has been corrected by normalizing the positions of the two maxima at one *pd* and one current. This correction, which is within the experimental uncertainty in establishing the positions of the electrodes, has been sufficient to bring all the data into excellent agreement.

While the thickness of the cathode fall, as given by the field profile, is close to that determined from the peak of excitation, it is systematically higher by approximately 0.02 cm. This difference is, however, well within the experimental uncertainty (and possibly within the uncertainty of the interpolation of the sheath electric field to zero). Nevertheless, the systematic difference exists and may be significant under some circumstances.

Considering all *pd* values, the length of the cathode sheath d_c closely follows the scaling relation

$$pd_c \propto (I/p^2)^{-0.26}, \tag{6}$$

as shown in Figure 10. This behavior is very similar to that found earlier for an Ar discharge with a copper cathode mounted inside a six-way metal cross that itself served as anode [28] (where the scaling exponent was found to be -0.2).

5 Conclusion

The volt-ampere characteristics and axial light emission profiles of argon glow discharges in the normal and abnormal mode, between plane-parallel electrodes have been investigated experimentally. Using the experimental electrical data the discharge has been described by a one-dimensional hybrid model, which made it possible to calculate the spatial distribution of light intensity (related to the electron impact excitation rate) allowing detailed comparison with the experimental data.

We have obtained excellent agreement between the experimental data and the results of the simulations in terms of the axial emission profiles. Such a comparison of *spatially resolved* data is a strong test of the applicability of the model. The model also made it possible to determine the apparent secondary electron yield in the discharges for a wide range of operating conditions. The apparent electron yield data as a function of the reduced electric field at the cathode agree reasonably with previous values of γ, obtained in a different way [23]. The apparent γ has been found to change by a factor of 2 for the discharge conditions covered here. Thus our procedure to modify γ to match the experimental and calculated volt-ampere curves is expected to give a more accurate description of the discharge, compared to any model that uses a pre-defined constant value for γ.

The only mismatch between the axial profiles that we have found occurs for the highest *pd* value where constriction of the discharge is significant at low currents, and may be associated with the one-dimensional nature of the model. At even higher *pd* values the constrictions will be even more pronounced and one may have to use a two-dimensional model for an accurate description of the discharge.

The position of the electric field reversal is found to be in excellent agreement with the predictions of the simple analytical model of Boeuf and Pitchford [37]. In addition to the more extensive comparisons of the hybrid model with experimental data and the analysis of the secondary electron yields, the present data give strong support to the usual assumption that the position of the peak of emission coincides with the edge of the cathode fall region. These results, however, may be questioned under more extreme conditions when step-wise excitation becomes dominant as has been shown in case of rf discharges [38].

The authors wish to acknowledge contribution of I. Stefanović, J. Živković and S. Živanov in the development of experimental technique and procedure used here. We also acknowledge discussions with A.V. Phelps, S. Vrhovac, and L.C. Pitchford, as well as the partial support from MNTRS (1478) and the Hungarian Scientific Research Found (OTKA-T-34156).

References

1. A.V. Phelps, Z.Lj. Petrović, B.M. Jelenković, Phys. Rev. E **47**, 2825 (1993)
2. Z.Lj. Petrović, I. Stefanović, S. Vrhovac, J. Živković, J. Phys. IV France **7**, C4-3412 (1997)

3. A.V. Phelps, Z.Lj. Petrović, Plasma Sources Sci. Technol. **8**, R21 (1999).
4. Z.Lj. Petrović, A.V. Phelps, Phys. Rev. E **47**, 2806 (1993)
5. Z.Lj. Petrović, A.V. Phelps, Proc. IEEE Plasma Sci. **24**, 107 (1996)
6. Z.Lj. Petrović, A.V. Phelps, Phys. Rev. E **56**, 5920 (1997)
7. B.M. Jelenković, K. Rózsa, A.V. Phelps, Phys. Rev. E **47**, 2816 (1993)
8. I. Stefanović, Z.Lj. Petrović, Jpn J. Appl. Phys. **36**, 4728 (1997)
9. P. Hartmann, Z. Donkó, G. Bánó, L. Szalai, K. Rózsa, Plasma Sources Sci. Technol. **9**, 183 (2000)
10. S. Živanov, J. Živković, I. Stefanović, S. Vrhovac, Z.Lj. Petrović, Eur. Phys. J. AP **11**, 59 (2000)
11. M. Radmilović, Z.Lj. Petrović, Eur. Phys. J. AP **11**, 35 (2000); V.Lj. Marković, S.R. Gocić, S.N. Stamenković, Z.Lj. Petrović, M. Radmilović, Eur. Phys. J. AP **14**, 171 (2001)
12. S. Živanov, G. Malović, A. Strinić, Z.Lj. Petrović, Europhys. Conf. Abst. **24F**, 134 (2000)
13. G. Auday, Ph. Guillot, J. Galy, H. Brunet, J. Appl. Phys. **83**, 5917 (1998)
14. G. Auday, Ph. Guillot, J. Galy, J. Appl. Phys. **88**, 4871 (2000)
15. R.A. Langley, J. Bohdansky, E. Eckstein, P. Mioduszevski, J. Roth, E. Taglauer, E.W. Thomas, H. Verbeek, K.L. Wilson, Nucl. Fusion, Special Issue, "Data Compendium for plasma-surface interactions", IAEA, Wienna, 1984
16. J.P. Boeuf, L.C. Pitchford, IEEE Trans. Plasma Sci. **19**, 286 (1991)
17. A. Fiala, L.C. Pitchford, J.P. Boeuf, Phys. Rev. E **49**, 5607 (1994)
18. A. Bogaerts, R. Gijbels, W.J. Goedheer, J. Appl. Phys. **78**, 2233 (1995); A. Bogaerts, R. Gijbels, J. Appl. Phys. **78**, 6427 (1995); A. Bogaerts, R. Gijbels, W. Goedheer, Jpn J. Appl. Phys. **38**, 4404 (1999)
19. Z. Donkó, Phys. Rev. E **57**, 7126 (1998)
20. V.V. Serikov, K. Nanbu, J. Appl. Phys. **82**, 5948 (1997)
21. I. Pérés, L.C. Pitchford, J. Appl. Phys. **78**, 774 (1995)
22. A.V. Phelps, L.C. Pitchford, C. Pédoussat, Z. Donkó, Plasma Sources Sci. Technol. **8**, B1 (1999)
23. Z. Donkó, Phys. Rev. E **64**, 026401 (2001)
24. K. Kutasi, Z. Donkó, J. Phys. D **33**, 1081 (2000)
25. K. Kutasi, P. Hartmann, Z. Donkó, J. Phys. D **34**, 3368 (2001)
26. M.J. Kushner, J. Appl. Phys. **54**, 4958 (1983); J.P. Boeuf, Phys. Rev. A **36**, 2782 (1987); N. Nakano, N. Shimura, Z.Lj. Petrović, T. Makabe, Phys. Rev. E. **49**, 4455 (1994)
27. Z.Lj. Petrović, Z. Donkó, D. Marić, G. Malović, S. Živanov, IEEE Trans. Plasma Sci. **30**, 136 (2002)
28. K. Rózsa, A. Gallagher, Z. Donkó, Phys. Rev. E **52**, 913 (1995)
29. A.L. Ward, J. Appl. Phys. **33**, 2789 (1962).
30. A.V. Phelps, Collision data compilation, `http://jilaweb.colorado.edu/www/research/colldata.html`
31. E.H. Darlington, V.E. Cosslett, J. Phys. D **5**, 1969 (1972)
32. E.J. Sternglass, Phys. Rev. **95**, 345 (1954)
33. A. Bogaerts, R. Gijbels, J. Vlcek, J. Appl. Phys. **84**, 121 (1998)
34. S. Živanov, D. Marić, Z.Lj. Petrović, *Proc. XX SPIG 2000*, edited by Z.Lj. Petrović, M.M. Kuraica, N. Bibić, G. Malović, p. 352, Zlatibor, 2000
35. A. Bogaerts, R. Gijbels, Plasma Sources Sci. Technol. **11**, 27 (2002)
36. A.V. Phelps, Plasma Sources Sci. Technol. **10**, 329 (2001)
37. J.P. Boeuf, L.C. Pitchford, J. Phys. D: Appl. Phys. **28**, 2083 (1995)
38. Z.Lj. Petrović, S. Bzenić, J. Jovanović, S. Djurović, J. Phys. D **28**, 2287 (1995)